Composite Interpolated Fast Fourier Transform With the Hanning Window

Kui Fu Chen and Shu Li Mei

***Abstract*—The composite interpolated fast Fourier transform (IpFFT) with the Hanning window is investigated to decrease the estimation variance. This form of composite IpFFT makes use of four consecutive spectral lines around a spectral peak. These four consecutive lines render three estimators using the complex spectrum-based interpolation. The three estimators can be averaged to decrease the variance, and their weighting coefficients are established to produce the minimum variance. Theoretical analysis shows that this composite IpFFT has its best performance under noncoherent sampling conditions, achieving a minimum frequency variance of 1.8 folds of the Cramér–Rao bound (CRB). The worst case occurs in the situation of coherent sampling, with a maximum variance of 2.6 folds of the CRB. Theoretical analysis was validated by numerical experiments on three types of noise-contaminated signals, cisoids, real-valued sine waves, and double-tone complex-valued signals. The cisoid case shows that the empirical variance very well matches the theoretical expression. Insofar as simulation is concerned (signal-to-noise ratio down to -2 dB), the empirical variance deviating from the theoretical expression is no more than 25%. All three experiments show that the empirical variance of the IpFFT is almost independent of the initial phase, whereas the bias is the opposite.**

***Index Terms*—Fast Fourier transforms (FFT), frequency estimation, least-mean-square methods, parameter estimation, spectrum analysis.**

I. Introduction

ESTIMATING parameters (frequency, amplitude, and phase) of sinusoids embedded in random noise has been the subject of many references from various fields for several decades [1]. The spectral analysis based on the fast Fourier transform (FFT) is extensively used in this community [2]. However, the canonical FFT has two error sources: 1) the spectral leakage due to time limitation and 2) the picket fence effect (PFE) due to discrete frequencies in the calculated spectrum [3]–[5]. Theoretically, even for a cisoid (complex sinusoid), the maximum biases of the amplitude and phase can be up to 36.3% and 90°, respectively [6], [7]. The interpolated FFT (IpFFT) was proposed to eliminate the PFE [8], [9].

Manuscript received November 5, 2008; revised June 4, 2009. Current version published May 12, 2010. This work was supported in part by the Natural Science Foundation of China under Grant 60772038. The Associate Editor coordinating the review process for this paper was Dr. Rik Pintelon.

K. F. Chen is with the College of Sciences, China Agricultural University, Beijing 100094, China (e-mail: ChenKuiFu@gmail.com).

S. L. Mei is with the College of Information and Electrical Engineering, China Agricultural University, Beijing 100083, China (e-mail: MeiShuLi@163.com).

Color versions of one or more of the figures in this paper are available online at http://ieeexplore.ieee.org.

Digital Object Identifier 10.1109/TIM.2009.2027772

It has been shown that the IpFFT [9] is subjected to a significant bias in a nearly coherent sampling condition [10], which is due to the incorrect interpolating direction [11]. The bias can appropriately be suppressed by windowing, for example, using the Hanning window by Grandke [12] or other cosine windows by Offelli and Petri [13], but at a cost of an increased variance [10], [14]. The variance can be reduced by some degree by using the phase information of a third spectral line, as proposed by Quinn [15], [16]. Aboutanios and Mulgrew improved the IpFFT performance by frequency shifting and iteration [17]. In the multitone or interharmonic cases, the *spectral leakage* occurring with the IpFFT must be considered too [18]. Liguori *et al.* have systematically studied this problem [19]. Agrež proposed the *weighted multipoint interpolated* FFT to suppress the spectral leakage [20]. Belega and Dallet extended this idea to a more general form [21].

To decrease the estimation variance, Quinn proposed a three-line estimator [22]. Macleod has given three- and five-line interpolators with a nearly optimal estimation variance [11]. It must be pointed out that both works of Quinn [22] and Macleod [11] did not involve windowing. Nonetheless, windowing is extensively used to suppress the spectral leakage [23], [24].

In this paper, we will consider the IpFFT with the Hanning window. Four discrete spectral lines around a peak are used to render three estimators. It will be shown that, by using an optimal average of the three estimators, the proposed composite IpFFT has a theoretical estimation variance of 1.77–2.63 folds of the Cramér–Rao bounds (CRBs). The theoretical analysis will be corroborated by the numerical simulation.

II. Complex Spectrum-Based FFT Interpolation

A. Interpolated FFT

The cisoid $x(t_i)$ contaminated with additive complex white noise is given as follows:

$$y(t_i) = x(t_i) + z(t_i) \tag{1}$$

where $z(t_i) = z_R(t_i) + jz_I(t_i)$ ($t_i = i\Delta T$, $i = 0$ to $N-1$, and ΔT and N are the sampling interval and size, respectively) is the discrete complex noise sequence. Both the real part $z_R(t_i)$ and the imaginary part $z_I(t_i)$ are real-valued discrete white noise with variance σ^2. Furthermore, we assume that the real and imaginary parts are independent of each other. The noise-free component $x(t_i)$ is

$$x(t_i) = A_0 \exp(j\omega_0 t_i + j\varphi_0) \tag{2}$$

where A_0, φ_0, and ω_0 are the amplitude, phase, and circular frequency of interest, respectively.

The Hanning window is

$$w(t)=\begin{cases}\frac{1-\cos(2\pi t/T)}{2}=\frac{1-\cos(\Delta\omega t)}{2}, & 0\le t\le T\\ 0, & t<0 \text{ or } t>T\end{cases} \quad (3)$$

where $T=N\Delta T$. In (3), $\Delta\omega=2\pi/T$ is the frequency resolution of the canonical FFT [2]. With the Hanning window, the discrete Fourier transform (DFT) of $y(t_i)$ is

$$Y(\omega)=X(\omega)+Z(\omega) \quad (4)$$

where $Z(\omega)$ is the DFT of $z(t_i)$ weighted by the Hanning window as

$$Z(\omega)=\sum_{i=0}^{N-1} w(t_i)z(t_i)\exp(-j\omega t_i). \quad (5)$$

The DFT of $x(t_i)$ in (4) is

$$X(\omega)=\sum_{i=0}^{N-1} A_0 w(t_i)\exp(j\omega_0 t_i+j\varphi_0)\exp(-j\omega t_i). \quad (6)$$

It can explicitly be expressed as

$$X(\omega)=-\pi m\left[\left(\sin\frac{\pi d}{N}\right)^{-1}-\frac{1}{2}\left(\sin\frac{\pi d-\pi}{N}\right)^{-1}-\frac{1}{2}\left(\sin\frac{\pi d+\pi}{N}\right)^{-1}\right] \quad (7)$$

where

$$d=(\omega_0-\omega)/\Delta\omega \quad (8)$$

$$m=-A_0\sin(\pi d)\exp\left[j\varphi_0+j\pi d(1-N^{-1})\right]/(2\pi). \quad (9)$$

First, N is generally far greater than 1, for example, $N=1024$. Second, only the spectrum lines around the main lobe are used in the IpFFT, where d/N is small. Consequently, $\sin(\pi d/N)\approx\pi d/N$, and $\sin[(\pi\pm1)d/N]\approx(\pi\pm1)d/N$. Taking into account both factors, (7) at the lth spectral line ω_l can be rewritten as

$$X_l=X(\omega_l)\approx Nm/\left[(d-1)d(d+1)\right]. \quad (10)$$

Since N is assumed to be large, then $N^{-1}\approx 0$. Accordingly,

$$m\approx -A_0\sin(\pi d)\exp(j\varphi_0+j\pi d)/(2\pi). \quad (11)$$

In practice, (4) is sped up by the FFT, where the frequency sampling interval is $\Delta\omega=2\pi/T$. Note that ω at an FFT spectral line is equal to an integer ν folds of $\Delta\omega$; thus, $d=\omega_0/\Delta\omega-\nu$ from (8). In this case, (11) becomes

$$\begin{aligned}m&\approx -\frac{A_0}{2\pi}\sin\pi\left(\frac{\omega_0}{\Delta\omega}-\nu\right)\exp\left[j\varphi_0+j\pi\left(\frac{\omega_0}{\Delta\omega}-\nu\right)\right]\\&=-\frac{A_0}{2\pi}\sin\left(\frac{\pi\omega_0}{\Delta\omega}\right)(-1)^{\nu}\exp\left(j\varphi_0+j\frac{\pi\omega_0}{\Delta\omega}\right)(-1)^{\nu}\\&=-\frac{A_0}{2\pi}\exp\left(j\varphi_0+j\frac{\pi\omega_0}{\Delta\omega}\right)\sin\left(\frac{\pi\omega_0}{\Delta\omega}\right).\end{aligned} \quad (12)$$

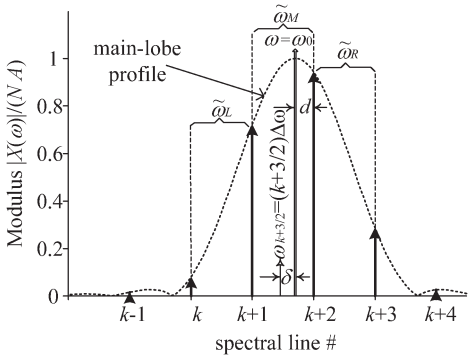

Fig. 1. Spectral lines around the main lobe.

This equation indicates that m is independent of the spectral line index ν.

It is due to the simplicity of (10) and (12) that there exists a simple closed-form interpolation formula for frequency ω_0.

With any two consecutive spectral lines l and $l+1$ close to the main lobe, it can be derived that [25], [26]

$$\omega_0=\omega_{l+1/2}+\frac{3}{2}\frac{X_{l+1}+X_l}{X_{l+1}-X_l}\Delta\omega \quad (13)$$

where $\omega_{l+1/2}=(l+1/2)\Delta\omega$. If X_l is replaced with the noise counterpart $Y_l=Y(l\Delta\omega)$, then (13) becomes an estimator. To ensure a real ω_0, the following estimator is adopted:

$$\tilde{\omega}_0=\omega_{l+1/2}+\frac{3}{2}\mathrm{Re}\left[\frac{Y_{l+1}+Y_l}{Y_{l+1}-Y_l}\right]\Delta\omega \quad (14)$$

where $\mathrm{Re}[\,]$ stands for the real part of a complex number. Another reason for using only the real part is that, for any complex random variable r, the variance of the real part is no greater than that of the absolute value, that is, $E[(\mathrm{Re}(r))^2]\le E[(\mathrm{Re}(r))^2]+E[(\mathrm{Im}(r))^2]=E[|r|^2]$.

B. Taylor Series Expansion

For statistical analysis, substituting (4) into (14) leads to

$$\tilde{\omega}_0=\omega_{l+1/2}+\frac{3}{2}\mathrm{Re}\left[\frac{X_{l+1}+X_l+Z_{l+1}+Z_l}{X_{l+1}-X_l+Z_{l+1}-Z_l}\right]\Delta\omega. \quad (15)$$

With the Hanning window and noncoherent sampling, there are four DFT spectral lines inside the window spectrum main lobe (cf. Fig. 1). To make use of symmetry, the central frequency $\omega_{k+3/2}=(k+3/2)\Delta\omega$ between the lines $k+1$ and $k+2$ is taken as the reference point.

The following dimensionless quantities are introduced to simplify derivation:

$$\begin{aligned}\delta_l&=(\omega_0-\omega_{k+3/2})/\Delta\omega-l/2\\&=(\omega_0-\omega_{k+1})/\Delta\omega-(l+1)/2\end{aligned} \quad (16)$$

where $\omega_{k+1}=(k+1)\Delta\omega$ (noting that ω_0 is defined after (2), instead of $0\Delta\omega$).

For facilitating variance analysis and optimal averaging in the ensuing paragraphs, we make an assumption as follows: The noise root-mean-square value σ is significantly less than A_0 in

the sense of probability. Retaining Taylor series expansion to the first order, (15) can be approximated as

$$\tilde{\omega}_0 \approx \omega_0 + 3\mathrm{Re}\left[\frac{-\delta_{2k-2l+1}Z_{l+1} + \delta_{2k-2l-5}Z_l}{X_{l+1} - X_l}\right]\Delta\omega. \quad (17)$$

III. Variance Analysis of the Composite Estimator

Any two consecutive spectral lines can be selected to estimate the frequency ω_0 by (15). For example, the spectral lines $k+1$ and $k+2$ embracing ω_0 give a frequency estimator, which is denoted in the ensuing paragraphs by $\tilde{\omega}_M$ because it is in the middle of two other estimators $\tilde{\omega}_L$ and $\tilde{\omega}_R$ depicted together in Fig. 1. $\tilde{\omega}_L$ and $\tilde{\omega}_R$ make use of line pairs $(k, k+1)$ and $(k+2, k+3)$, respectively, and their subscripts L and R denote their individual positions being on the left and right sides of $\tilde{\omega}_M$ in Fig. 1.

Now, we consider the variance of the following composite estimator:

$$\tilde{\omega} = \beta_L\tilde{\omega}_L + \beta_R\tilde{\omega}_R + (1 - \beta_L - \beta_R)\tilde{\omega}_M \quad (18)$$

where β_L, β_R, and $(1 - \beta_L - \beta_R)$ are weighting coefficients. β_L and β_R have to be optimized for a minimum variance.

Applying (14) to the three individual estimators is embodied as

$$\left.\begin{aligned}\tilde{\omega}_L &= \omega_0 + 3\mathrm{Re}\left[\tfrac{-\delta_1 Z_{k+1} + \delta_{-5}Z_k}{X_{k+1} - X_k}\right]\Delta\omega \\ \tilde{\omega}_M &= \omega_0 + 3\mathrm{Re}\left[\tfrac{-\delta_3 Z_{k+2} + \delta_{-3}Z_{k+1}}{X_{k+2} - X_{k+1}}\right]\Delta\omega \\ \tilde{\omega}_R &= \omega_0 + 3\mathrm{Re}\left[\tfrac{-\delta_5 Z_{k+3} + \delta_{-1}Z_{k+2}}{X_{k+3} - X_{k+2}}\right]\Delta\omega\end{aligned}\right\}. \quad (19)$$

Substituting (19) into (18) leads to

$$\tilde{\omega}_0 = \omega_0 + \mathrm{Re}(\lambda_L\beta_L + \lambda_R\beta_R + \lambda) \quad (20)$$

where

$$\left.\begin{aligned}\lambda_L &= \gamma\delta_{-3}\left[\delta_{-5}^2 Z_k + 2(2 - \delta_{-1}^2)Z_{k+1} + \delta_3^2 Z_{k+2}\right] \\ \lambda_R &= -\gamma\delta_3\left[\delta_{-3}^2 Z_{k+1} + 2(2 - \delta_1^2)Z_{k+2} + \delta_5^2 Z_{k+3}\right] \\ \lambda &= \gamma\delta_3\delta_{-3}(\delta_{-3}Z_{k+1} - \delta_3 Z_{k+2})\end{aligned}\right\}$$
$$\gamma = (1 - 4\delta^2)\Delta\omega/(4m) \quad (21)$$

where $\delta(=\delta_0)$ is the shift of the frequency ω_0 from $\omega_{k+3/2}$ in the unit of $\Delta\omega$.

Since the mean value of Z_k is zero in light of (5), the estimator $\tilde{\omega}_0$ of (20) is nonbiased, i.e.,

$$E[\tilde{\omega}_0] \approx \omega_0. \quad (22)$$

In light of the derivation in the Appendix in [27], the variance of (20) is

$$\begin{aligned}\sigma_{\omega_0}^2 &= E\left[\mathrm{Re}(\lambda_L\beta_L + \lambda_R\beta_R + \lambda)^2\right] \\ &= E\left[|\lambda_L\beta_L + \lambda_R\beta_R + \lambda|^2\right]/2. \end{aligned} \quad (23)$$

It can further be written as

$$\begin{aligned}\sigma_{\omega_0}^2 = \{&\beta_L^2 E\left[|\lambda_L|^2\right] + \beta_R^2 E\left[|\lambda_R|^2\right] + 2\beta_L\beta_R\mathrm{Re}(E[\lambda_L\lambda_R^*]) \\ &+ 2\beta_L\mathrm{Re}(E[\lambda_L\lambda^*]) + 2\beta_R\mathrm{Re}(E[\lambda_R\lambda^*]) + E\left[|\lambda|^2\right]\}/2. \end{aligned} \quad (24)$$

Now, we turn to $E[|\lambda_L|^2]$. In light of the first formula of (21), it can be reformulated as

$$\begin{aligned}E\left[|\lambda_L|^2\right] &= |\gamma\delta_{-3}|^2\Big\{\delta_{-5}^4 E\left[|Z_k|^2\right] + 4\left(2 - \delta_{-1}^2\right)^2 E\left[|Z_{k+1}|^2\right] \\ &\quad + \delta_3^4 E\left[|Z_{k+2}|^2\right] + 2\delta_{-5}^2\left(2 - \delta_{-1}^2\right) \\ &\quad \times E\left[\mathrm{Re}\left(Z_k Z_{k+1}^*\right)\right] + 2\delta_{-5}^2\delta_3^2 E\left[\mathrm{Re}\left(Z_k Z_{k+2}^*\right)\right] \\ &\quad + 4\left(2 - \delta_{-1}^2\right)\delta_3^2 E\left[\mathrm{Re}\left(Z_{k+1}Z_{k+2}^*\right)\right]\Big\}. \end{aligned} \quad (25)$$

The covariance between the windowed FFT spectral lines is evaluated in the Appendix. Substituting them in (25) leads to

$$E\left[|\lambda_L|^2\right] = 2\mu(3 + 2\delta)^2\Psi(\delta) \quad (26)$$

where

$$\left.\begin{aligned}\Psi(\delta) &= 1027 + 2200\delta + 2760\delta^2 + 1120\delta^3 + 560\delta^4 \\ \mu &= \tfrac{|\gamma|^2}{512}\tfrac{\sigma^2}{N}\Delta^2\omega = \tfrac{(1-4\delta^2)^2}{8192|m|^2}\tfrac{\sigma^2}{N}\Delta^2\omega \\ &= \tfrac{\pi^2\sigma^2(1-4\delta^2)^2}{2048N^3A^2\cos^2(\pi\delta)}\Delta^2\omega\end{aligned}\right\}. \quad (27)$$

Similarly, we have

$$\left.\begin{aligned}E\left[|\lambda_R|^2\right] &= 2\mu(3-2\delta)^2\Psi(-\delta) \\ E\left[|\lambda|^2\right] &= 4\mu(9+20\delta^2)(9-4\delta^2)^2 \\ E\left[\mathrm{Re}\left(\lambda_L\lambda_R^*\right)\right] &= -8\mu(9-4\delta^2)(87+360\delta^2+112\delta^4) \\ E\left[\mathrm{Re}(\lambda_L\lambda^*)\right] &= \mu(3-2\delta)(3+2\delta)^2\Phi(\delta) \\ E\left[\mathrm{Re}(\lambda_R\lambda^*)\right] &= \mu(3+2\delta)(3-2\delta)^2\Phi(-\delta)\end{aligned}\right\} \quad (28)$$

where

$$\Phi(\delta) = 87 + 450\delta + 180\delta^2 + 280\delta^3. \quad (29)$$

IV. Optimization

A. Optimal Weighting

Equation (24) has two variables, i.e., β_L and β_R. The optimal values should be

$$\left\{\begin{aligned}\beta_{L,\min} &= \left\{E\left[|\lambda_R|^2\right]\mathrm{Re}\left(E[\lambda_L\lambda^*]\right)\right. \\ &\quad \left. - \mathrm{Re}\left(E\left[\lambda_L\lambda_R^*\right]\right)\mathrm{Re}\left(E[\lambda_R\lambda^*]\right)\right\}/D \\ \beta_{R,\min} &= \left\{E\left[|\lambda_L|^2\right]\mathrm{Re}\left(E[\lambda_R\lambda^*]\right)\right. \\ &\quad \left. - \mathrm{Re}\left(E\left[\lambda_L\lambda_R^*\right]\right)\mathrm{Re}\left(E[\lambda_L\lambda^*]\right)\right\}/D\end{aligned}\right. \quad (30)$$

where

$$D = \mathrm{Re}\left(E\left[\lambda_L\lambda_R^*\right]\right)^2 - E\left[|\lambda_L|^2\right]E\left[|\lambda_R|^2\right]. \quad (31)$$

As a result, the optimal variance is

$$\begin{aligned}\sigma_{\omega_0,\min}^2 = E\left[|\lambda|^2\right]/2 + D^{-1}\Big\{&E\left[|\lambda_R|^2\right]\left(\mathrm{Re}\left(E[\lambda_L\lambda^*]\right)\right)^2 \\ &+ E\left[|\lambda_L|^2\right]\left(\mathrm{Re}\left(E[\lambda_R\lambda^*]\right)\right)^2 \\ &- 2\mathrm{Re}\left(E\left[\lambda_L\lambda_R^*\right]\right)\mathrm{Re}\left(E[\lambda_L\lambda^*]\right) \\ &\times \mathrm{Re}\left(E[\lambda_R\lambda^*]\right)\Big\}/2. \end{aligned} \quad (32)$$

Substituting (26)–(29) into (30) leads to

$$\left\{\begin{aligned}\beta_{L,\min} &= (2\delta - 5)(2\delta - 3)\kappa_L(\delta)/\kappa \\ \beta_{R,\min} &= (2\delta + 5)(2\delta + 3)\kappa_R(\delta)/\kappa\end{aligned}\right. \quad (33)$$

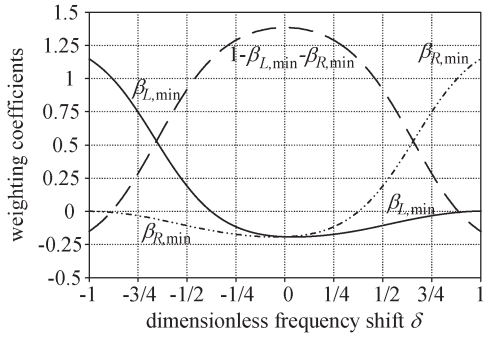

Fig. 2. Dependence of weighting coefficients on δ.

where

$$\begin{cases} \kappa_R(\delta) = \kappa_L(-\delta) \\ \qquad = 15\,680\delta^6 + 26\,880\delta^5 + 42\,000\delta^4 \\ \qquad\quad + 33\,152\delta^3 + 62\,460\delta^2 + 32\,400\delta - 23\,925\,. \\ \kappa = 2(112\,896\delta^8 + 546\,560\delta^6 + 1\,454\,432\delta^4 \\ \qquad - 173\,200\delta^2 + 933\,625) \end{cases} \quad (34)$$

The dependence of $\beta_{L,\min}$ and $\beta_{R,\min}$ on δ is presented in Fig. 2. Inspecting this figure, we have four remarks.

1) If δ is around zero, then the weight of ω_M is significantly greater than those of ω_L and ω_R, since ω_M is more accurate than ω_L and ω_R. When $\delta = 0$, $\beta_{L,\min} = \beta_{R,\min} = -261/1358 < 0$; consequently, the weight of ω_M, i.e., $1 - \beta_{L,\min} - \beta_{R,\min}$, is greater than 1.
2) As δ deviates from zero to the right, $\beta_{R,\min}$ increases, whereas the weight of ω_M decreases. The absolute value of $\beta_{L,\min}$ decreasing to zero indicates that the contribution of the left estimator ω_L dilutes.
3) The negative weights at some δ differ from the general impression given in textbooks, where they are usually nonnegative. This might be caused by a negative correlation among three considered frequency estimators. Most important, it indicates that weights cannot arbitrarily be chosen.
4) The optimal weights depend on δ, but the latter is the estimation objective. Thus, we have to achieve the pseudooptimal weights beforehand. One recipe is taking a coarse δ using the first and second highest spectra as two-line interpolation.

B. Optimal Variance

Substituting (26)–(28) into (32) leads to

$$\sigma^2_{\omega_0,\min} = \frac{\pi^2\sigma^2\Delta^2\omega}{18\,432NA^2}\frac{(1-4\delta^2)^2(9-4\delta^2)^2(25-4\delta^2)^2}{\kappa\cos^2(\pi\delta)} \times(15\,680\delta^6 - 34\,384\delta^4 + 57\,260\delta^2 + 37\,125). \quad (35)$$

This optimal variance varying as δ is illustrated in Fig. 3. In the figure, the variances are scaled by the following CRB [28]:

$$\omega^2_{\mathrm{CRB}} = \frac{12\sigma^2}{N^3A^2\Delta^2T} = \frac{3\sigma^2\Delta^2\omega}{\pi^2NA^2}. \quad (36)$$

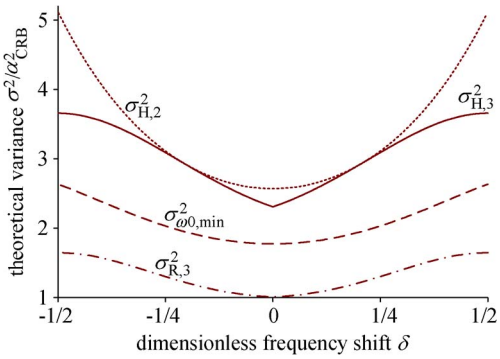

Fig. 3. Dependence of the optimal variance on δ.

For comparison, three lines showing the variances of other three different estimators are illustrated together. They are optimal variances of the IpFFT for the following cases:

1) $\sigma^2_{R,3}$ for three spectral lines with variance minimization but without windowing (rectangular window) [27];
2) $\sigma^2_{H,2}$ for two lines with the Hanning window [25];
3) $\sigma^2_{H,3}$ for three spectral lines with the Hanning window and variance minimization (3L-IpFFTVM) [25].

With the variable δ defined in this paper, their expressions are

$$\sigma^2_{H,2} = \frac{\pi^2\sigma^2\Delta^2\omega}{9216NA^2}\frac{(1-4\delta^2)^2(9-4\delta^2)^2(9+20\delta^2)}{\cos^2(\pi\delta)} \quad (37)$$

$$\sigma^2_{H,3} = \frac{5\pi^2\sigma^2\Delta^2\omega(5-2|\delta|)^2(1-4\delta^2)^2(9-4\delta^2)^2}{73\,728NA^2\cos^2(\pi\delta)} \times\frac{531-216|\delta|+776\delta^2-1120|\delta|^3+560\delta^4}{1027-2200|\delta|+2760\delta^2-1120|\delta|^3+560\delta^4} \quad (38)$$

$$\sigma^2_{R,3} = \frac{\pi^2\sigma^2\Delta^2\omega(3-2|\delta|)^2(1-4\delta^2)^2}{128NA^2\cos^2(\pi\delta)} \times\frac{19-24|\delta|+72\delta^2-96|\delta|^3+48\delta^4}{43-120|\delta|+168\delta^2-96|\delta|^3+48\delta^4}. \quad (39)$$

Fig. 3 shows that $\sigma^2_{\omega0,\min}$ has the lowest value at $\delta = 0$. The lowest value is $50\,625\pi^4/2\,781\,184\sigma^2_{\mathrm{CRB}} \approx 1.773\sigma^2_{\mathrm{CRB}}$, which is significantly lower than those of $\sigma^2_{H,2}$ and $\sigma^2_{H,3}$ ($2.568\sigma^2_{\mathrm{CRB}}$ and $2.306\sigma^2_{\mathrm{CRB}}$, respectively) in the same condition. The worst case occurs at $\delta = \pm 1/2$, i.e., the coherent sampling condition, where $\sigma^2_{\omega0,\min} = 258\pi^2/967\sigma^2_{\mathrm{CRB}} = 2.633\sigma^2_{\mathrm{CRB}}$. In the whole range of $|\delta| < 1/2$, $\sigma^2_{\omega0,\min}$ is 0.654–0.769 folds of $\sigma^2_{H,3}$.

This figure also indicates that the difference between $\sigma^2_{\omega0,\min}$ and $\sigma^2_{H,3}$ is more significant than that between $\sigma^2_{H,3}$ and $\sigma^2_{H,2}$, but the spectral line number increments from $\sigma^2_{H,2}$ to $\sigma^2_{H,3}$ and from $\sigma^2_{H,3}$ to $\sigma^2_{\omega0,\min}$ are the same, which are both 1.

It is worth noting that $\sigma^2_{\omega0,\min}$ is still significantly higher than $\sigma^2_{R,3}$, which is the optimal variance of the IpFFT with three spectral lines and the rectangular window [27]. The reason is that any specific windowing will increase the estimation variance. However, the spectral analysis with the rectangular window has significant leakage from neighboring spectral lines, which could cause significant bias, and should be cautioned in practical use.

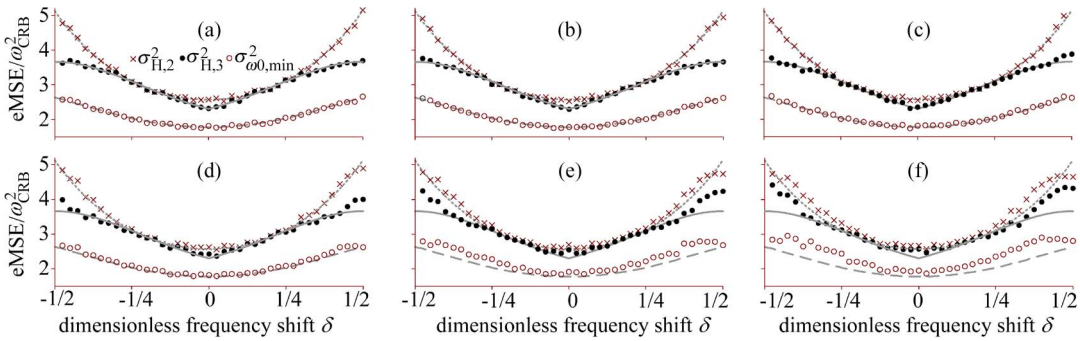

Fig. 4. Comparison between the empirical and theoretical variances for cisoids (theoretical variance line styles, cf. Fig. 3). (a) SNR = 50 dB. (b) SNR = 30 dB. (c) SNR = 10 dB. (d) SNR = 5 dB. (e) SNR = 0 dB. (f) SNR = 2 dB.

V. Numerical Simulation

Three experiments were conducted. The first experiment was to compare the empirical performance and theoretical analysis for the cisoid using three estimators, namely, the new four-line estimator, the two-line estimator, and the 3L-IpFFTVM [25]. The second and third experiments evaluated the bias and variance of the new estimator for real-valued sine waves and double-tone complex-valued signals. The purposes of the three experiments were different. The first experiment was to examine the variance deduction from the two-line estimator and the 3L-IpFFTVM to the new estimator, and the consistency between the numerical simulation and the theoretical analysis. The second and third experiments were to compare the new estimator with the recently developed multipoint IpFFT [21]. Therefore, the compared estimators, except the new one, were different between the first experiment and the second and third experiments.

A. Cisoid Cases

Equation (1) is used to generate time sequences. The amplitude A_0 is fixed at 1. The initial phase φ_0 does not appear in (33) and (35); thus, it is simulated as a random variable uniformly distributed on $[0, 2\pi]$ for any sequence. The sampling size is $N = 256$, and the interval is $\Delta t = 1$. The frequency ω_0 scans from $34.5\Delta\omega$ to $35.5\Delta\omega$ by a step $0.025\Delta\omega$. The added noise is white Gaussian with zero mean. Six levels of the SNR [SNR $= 20\ \lg(A_0/\sigma)$], i.e., 50, 30, 10, 5, 0, and -2 dB, were examined. For each combination of the frequency $\times$ SNR, 10 000 replications of sequences were carried out. Three approaches of the IpFFT, i.e., the two-line estimator, the 3L-IpFFTVM [25], and the present four-line estimator, are compared here. The coarse δ used to compute the optimal weight for the three- and four-line approaches is based on the two-line approach applied to the first and second highest lines. The ensuing second and third experiments adopt the same procedure.

The empirical mean square errors (eMSEs), which are calculated as in [29], are shown in Fig. 4. (The empirical bias is close to zero, as indicated in (22); hence, it is not shown.) This figure indicates that the eMSEs of all three approaches follow the theoretical variance (the continuous gray lines, cf. Fig. 3) at a higher SNR case [Fig. 4(a) and (b)]. As the SNR decreases [Fig. 4(c) and (d)], $\sigma^2_{H,3}$ deviates by a small degree from the theoretical variance when sampling is near the coherent condition ($\delta = \pm 1/2$).

In Fig. 4(e) and (f), i.e., the low-SNR cases (0 and -2 dB), all three variances mildly deviate from the theoretical variances. However, even for the worst case in Fig. 4(f), the maximum deviation of the new estimator is only about 25% of $\sigma^2_{\omega 0,\min}$. This deviation is probably due to approximations involved in derivation from (15)–(17), where a high SNR is assumed.

B. Real-Valued Sine Waves

The signals are generated as follows:

$$y(t_i) = A_0 \cos(\omega_0 t_i + \varphi_0) + z_R(t_i).$$

Only two levels of the SNR ($= 20\ \lg(A_0/\sigma) - 10\ \lg\ 2$, noting that it is different by about 3 dB compared with the cisoid case), i.e., 10 and 50 dB, are examined. Because several references emphasize that the IpFFT performance is dependent on initial phases [19], [20], therefore, four initial phases $\varphi = 0^\circ,\ 45^\circ,\ 90^\circ,$ and 135° were investigated. The frequency scans two segments, i.e., $3\Delta\omega$–$6\Delta\omega$ and $30\Delta\omega$–$31\Delta\omega$, by a step of $0.025\Delta\omega$. Other simulation parameters are the same as in the cisoid cases.

A real-valued sine wave is made up by two cisoids; however, the IpFFT is based only a single cisoid and ignores all other components. Therefore, the systematic error (or bias) definitely occurs. Accordingly, the eMSE is decomposed as eMSE $= \sigma_E^2 + b_E^2$ in Figs. 5 and 6, where σ_E and b_E are the empirical root variance and the bias over the 10 000 replications of sequences. σ_E and b_E are scaled by the frequency resolution $\Delta\omega$ of the canonical FFT for comparing their sizes. (Data in Figs. 3 and 4 are scaled by the CRB instead.)

Along with the new composite IpFFT in Figs. 5 and 6, three other IpFFTs were surveyed, which used two lines (2L-IpFFT) as in [12], three lines (3L-IpFFT), and five lines (5L-IpFFT). The 3L-IpFFT was proposed in [20] and was recently extended to the five-line case [21]. (Four spectral lines are used in this composite IpFFT, but the four-line IpFFT was not provided in [21].)

The top rows in Figs. 5 and 6 show that, first, the root variance of the composite IpFFT is the lowest of the four compared IpFFTs and is almost parallel to that of the 2L-IpFFT.

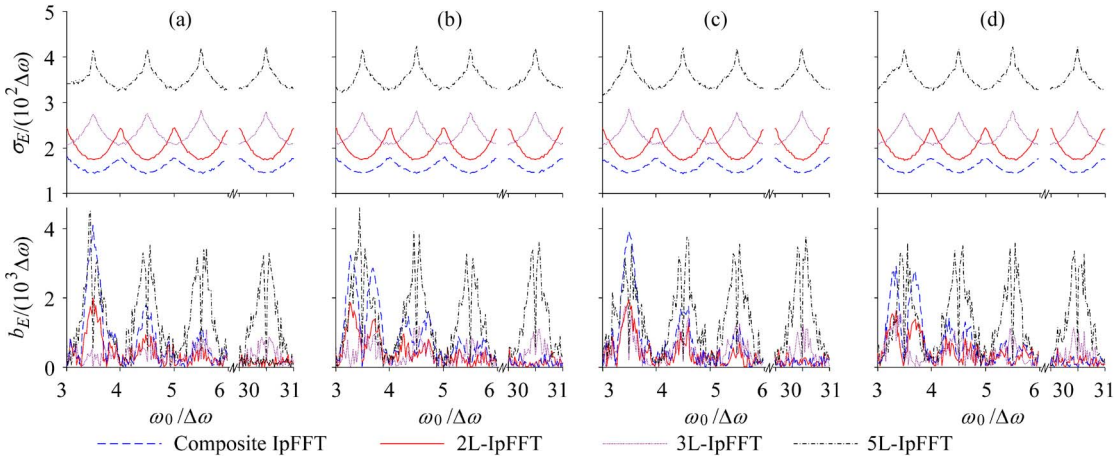

Fig. 5. Empirical variance and bias for real-valued sine waves contaminated by heavy noise (SNR = 10 dB). (a) $\varphi = 0°$. (b) $\varphi = 45°$. (c) $\varphi = 90°$. (d) $\varphi = 135°$.

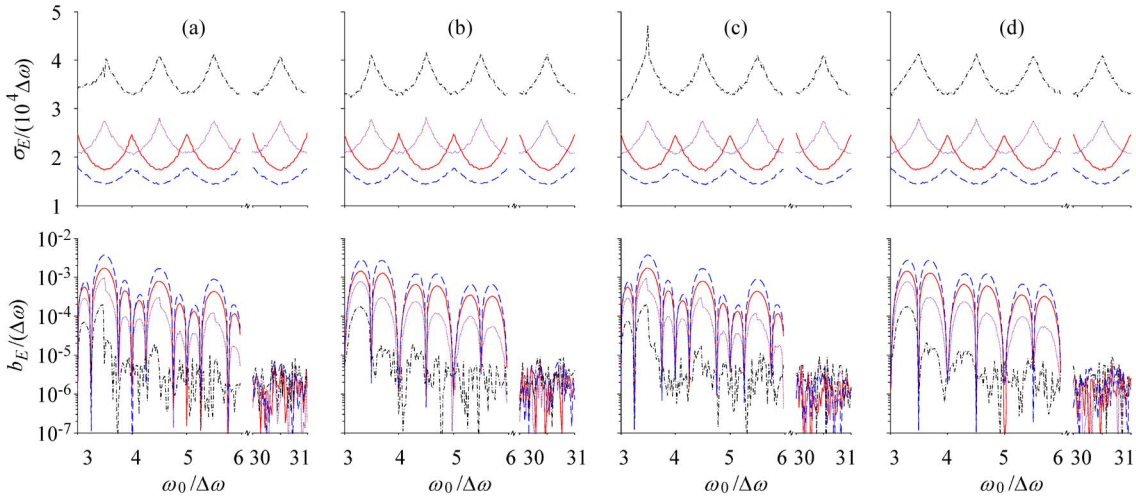

Fig. 6. Empirical variance and bias for real sine waves contaminated by weak noise (SNR = 50 dB) (line styles, cf. Fig. 5). (a) $\varphi = 0°$. (b) $\varphi = 45°$. (c) $\varphi = 90°$. (d) $\varphi = 135°$.

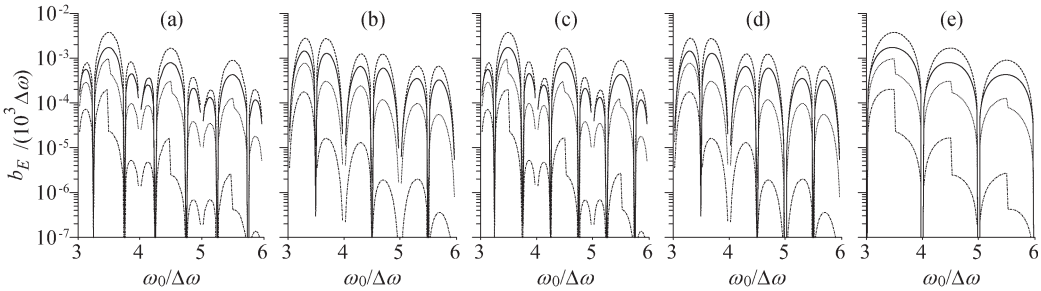

Fig. 7. Bias for real-valued sine waves free of noise (line styles, cf. Fig. 5). (a) $\varphi = 0°$. (b) $\varphi = 45°$. (c) $\varphi = 90°$. (d) $\varphi = 135°$. (e) envelope.

The 5L-IpFFT has the largest variance, and the root variance is at least twice that of the composite IpFFT.

Second, the root variance is independent of the initial phases to some degree (insofar as simulation is concerned) in both the lower (Fig. 5) and the higher (Fig. 6) SNR cases. Only the 5L-IpFFT is dependent on the initial phases if the frequency is low down to $3\Delta\omega$ (left end).

Third, the root variance with respect to the frequency is almost periodic with a period $\Delta\omega$. For the composite IpFFT and the 2L-IpFFT, the root variance has peaks at integer folds of $\Delta\omega$ and troughs at half-integer folds of $\Delta\omega$. This pattern does not vary as the frequency changes, from very low $3\Delta\omega{-}4\Delta\omega$ to very high $30\Delta\omega{-}31\Delta\omega$. In a basic period $\Delta\omega$, the patterns of the 3L-IpFFT and the 5P-IpFFT estimators are in-phase each other and in-quadrature with respect to the composite IpFFT and 2L-IpFFT estimators.

Fourth, as the SNR increases, σ_E decreases (comparing top rows in Figs. 5 and 6), but the bias b_E does not, particularly when ω_0 falls between $3\Delta\omega$ and $6\Delta\omega$. In addition, b_E is dependent on the initial phases. This is also corroborated by Fig. 7, where b_E for four initial phases are depicted in (a)–(d).

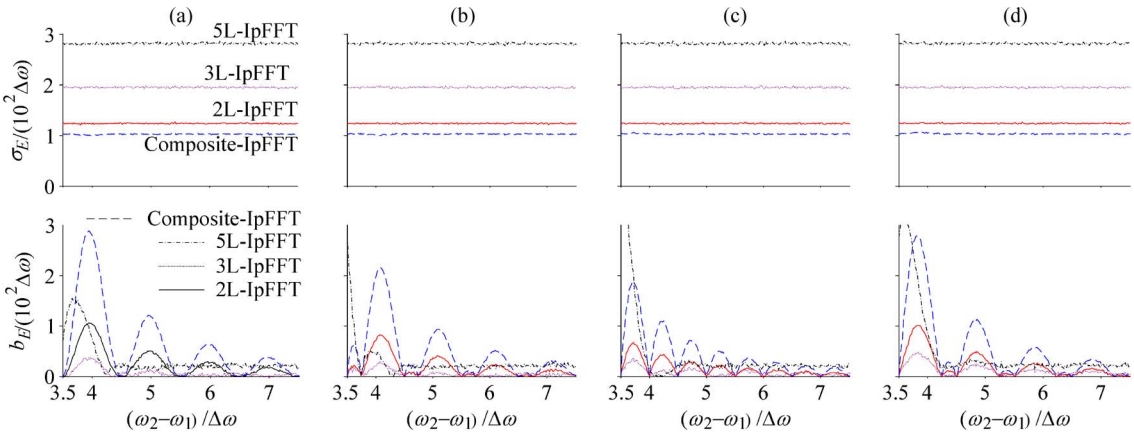

Fig. 8. Empirical variance and bias for the double-tone signal contaminated by strong noise (SNR = 10 dB) (line styles, cf. Fig. 5). (a) $\varphi = 0°$. (b) $\varphi = 45°$. (c) $\varphi = 90°$. (d) $\varphi = 135°$.

These observations can be argued as follows: The eMSE has two main sources. The first source is the random noise $z(t)$, and the second source is the spectral leakage from other tones. σ_E is mainly caused by the random noise, whereas b_E is mainly caused by the spectral leakage. In cisoid cases, b_E is close to zero because only one tone is embedded in noise.

When the SNR is higher (Fig. 6), the errors from two sources are separable (no interaction). The bias b_E is almost solely caused by the spectral leakage. In Fig. 7, b_E over $3\Delta\omega-6\Delta\omega$ is shown for the case of the real-valued sine wave free of noise. We can see the consistency between the bottom rows in Figs. 6 and 7(a)–(d). The spectral leakage is dependent on the initial phase, so is the bias b_E. In contrast, σ_E is almost independent of the initial phases in Figs. 5 and 6.

For a lower SNR case, it can be still expected that the bias b_E is dependent on the initial phase, whereas the correlation between the bottom rows of Figs. 5 and 7(a)–(d) is not very clear. This is likely due to the coupling interaction between the spectral leakage and the random noise. σ_E is independent of the initial phases in Fig. 5 because the random noise is dominated over the spectral leakage,

According to eMSE $= \sigma_E^2 + b_E^2$ and the foregoing simulation results, it follows that the eMSE depends on the initial phase when the SNR is high, whereas it is almost independent of the initial phase when the SNR is low (not shown).

Because the composite IpFFT is aimed to decrease the variance, it indeed has the best performance from the view of variance in both Figs. 5 and 6. The 3L-IpFFT and 5L-IpFFT are intended to suppress the effects of the spectral leakage, and they indeed achieve the target for a higher SNR case, as shown by the bottom row in Fig. 6. This can systematically be revealed by the error envelope for the noise-free wave in Fig. 7(e).

The error envelope is made as follows: At each frequency ω_0 scanning $3\Delta\omega-6\Delta\omega$ by a step $0.025\Delta\omega$, 180 initial phases (φ_0) linearly scan from 0° to 179° with a step 1°. All the errors from 180 initial phases are pooled together, and the ordinate in Fig. 7(e) is the maximum error among 180 initial phases at each frequency. This envelope provides the maximum error information pertaining solely to the spectral leakage.

It should be noted that, first, the bias maximum for all four kinds of the IpFFT is rather secondary, provided that ω_0 is no less than $3\Delta\omega$. The composite IpFFT has the largest error (less than $0.004\Delta\omega$) occurring around $3.5\Delta\omega$. Second, the global envelope trends decrease as ω_0 increases. Third, the 5L-IpFFT has the smallest envelope as intended. However, this advantage may be nullified under a low-SNR scenario. For example, the bottom row in Fig. 5 shows that the 5L-IpFFT has the largest bias when ω_0 is over $30\Delta\omega-31\Delta\omega$, which might be due to the interaction between the spectral leakage and the random noise.

C. Double-Tone Case

The interference between tones is caused by the spectral leakage. Without loss of generality, we examine tones with equal amplitudes here. Due to the decaying trait of the spectral leakage, the most severe interference must occur between two closest tones in frequency, and the spectral leakage from the third and other tones will be overridden by that from the closest tone (equal amplitude). Accordingly, the following double cisoid will be investigated:

$$y(t_i) = A_1 \exp(j\omega_1 t_i + j\varphi_1) + A_2 \exp(j\omega_2 t_i + j\varphi_2) + z(t_i).$$

Only a lower SNR, i.e., 10 dB, is examined, where the SNR is defined as $20\ \lg(A_1/\sigma)$. The lower tone ω_1 is fixed at $20.5\Delta\omega$ (corresponding to the most noncoherent sampling), and four initial phases, i.e., $\varphi_1 = 0°,\ 45°,\ 90°$ and 180°, are surveyed. The higher tone, i.e., ω_2, scans from $\omega_1 + 3.5\Delta\omega$ to $\omega_1 + 7.5\Delta\omega$ with a step of $0.02\Delta\omega$. Two initial phases, i.e., $\varphi_2 = 0°$ and 45°, are examined; however, only the case of $\varphi_2 = 0°$ is discussed (Fig. 8), because there is no significant difference between them.

Because of the symmetry between two tones, only the variance and bias for ω_1 are illustrated in Fig. 8. The interpolating lines for ω_1 center at $20.5\Delta\omega$ *a priori*, instead of selecting the local highest spectral line *ad hoc*. Other parameters are the same as for the cisoid case.

Fig. 8 indicates that, again, first, the composite IpFFT has the lower variance, and second, all the variances are almost independent of their own initial phase of φ_1. In fact, the

variance is also independent of φ_2, which is the initial phase of the tone considered as the spectral leakage origin (not shown).

The bias of the composite, 2L, and 3L-IpFFT diminishes as the separation between tones increases. However, the bias of the 5L-IpFFT does not significantly decrease as the tone separation changes from $5\Delta\omega$ to $7.5\Delta\omega$, although it has the best effect for the noise-free case.

VI. Conclusion

To decrease the estimation variance, we have investigated the composite IpFFT with the Hanning window. The success of the composite operation is due to the fact that complex spectra are used, instead of modulus, in the IpFFT. This way ensures that two spectral lines can produce rational frequency estimation, even if the true frequency is not trapped between the two spectral lines.

The four consecutive lines around a peak give three estimators. The optimal weight to combining the three estimators is derived. By optimal average, the proposed composite IpFFT has an estimation of 1.773–2.633 folds of the CRBs. The numerical experiment on the noise-contaminated cisoid shows that the empirical variance very well matches the theoretical expression. The new approach was compared with the traditional two-line IpFFT and the recently proposed three- and five-line IpFFTs on the noise-contaminated real-valued sine wave and the double-tone complex signal. It was demonstrated that the variance is almost independent of the tone's own initial phase and the parameters of other interfering tones, if the tone separation is greater enough. The bias depends on initial phases and tone separation.

If the random noise dominates over the spectral leakage, the composite IpFFT is preferred, whereas the 5L-IpFFT is a better choice when the spectral leakage from other tones is serious. How to balance between them needs further work [30], as well as a quantitative model for the spectral leakage.

The optimal weight for other windows will be developed in the future, although the work seems much involved. We need to also consider whether more than four lines can give significantly better deduction in the estimation variance, because the deduction from the $\sigma^2_{H,3}$ three-line estimator to $\sigma^2_{\omega 0,\min}$ is much greater than from $\sigma^2_{H,2}$ to $\sigma^2_{H,3}$ (cf. Fig. 3).

Appendix

For the windowed FFT of complex white noise, the following equations can derived [25], [30]:

$$E[Z_k Z_l] = 0 \text{ for any integer } l \text{ and } k \tag{A1}$$

$$E\left[Z_k Z_l^*\right] = 2\sigma^2 \sum_{i=0}^{N-1} w^2(t_i) \exp\left[-j(k-l)\Delta\omega t_i\right]. \tag{A2}$$

Substituting (2) in the main text into (A2) leads to

$$E\left[Z_k Z_l^*\right] = \frac{\sigma^2}{4} \sum_{i=0}^{N-1} \left\{[3 - 4\cos(\Delta\omega t_i) + \cos(2\Delta\omega t_i)] \times \exp\left[-j(\omega_k - \omega_l)t_i\right]\right\}. \tag{A3}$$

In light of the properties of triangular functions, (A3) can explicitly be reformulated as

$$E\left[Z_k Z_l^*\right] = \begin{cases} 3N\sigma^2/4, & l = k \\ -N\sigma^2/2, & l = k \pm 1 \\ N\sigma^2/8, & l = k \pm 2 \\ 0, & \text{for other } l \text{ and } k. \end{cases} \tag{A4}$$

Acknowledgment

The authors would like to thank S. Crowsen for his assistance with editing this paper.

References

[1] B. G. Quinn and E. J. Hannan, *The Estimation and Tracking of Frequency*. Cambridge, U.K.: Cambridge Univ. Press, 2001.
[2] J. W. Cooley and J. W. Tukey, "An algorithm for the machine computation of complex Fourier series," *Math. Comput.*, vol. 19, no. 90, pp. 297–301, 1965.
[3] Y. F. Li and K. F. Chen, "Eliminating the picket fence effect of the fast Fourier transform," *Comput. Phys. Commun.*, vol. 178, no. 7, pp. 486–491, Apr. 2008.
[4] H. A. Gaberson, "A comprehensive windows tutorial," *Sound Vib.*, vol. 40, no. 3, pp. 14–23, 2006.
[5] B. Rust, "The fast Fourier transform for experimentalists. Part III: Classical spectral analysis," *IEEE Comput. Sci. Eng.*, vol. 7, no. 5, pp. 74–78, Sep./Oct. 2005.
[6] M. Xie and K. Ding, "Corrections for frequency, amplitude and phase in a fast Fourier transform of a harmonic signal," *Mech. Syst. Signal Process.*, vol. 10, no. 2, pp. 211–221, Mar. 1996.
[7] I. Santamaria-Caballero, C. J. Pantaleon-Prieto, and J. Ibanez-Diaz, "Improved procedures for estimating amplitudes and phases of harmonics with application to vibration analysis," *IEEE Trans. Instrum. Meas.*, vol. 47, no. 1, pp. 209–214, Feb. 1998.
[8] D. C. Rife and G. A. Vincent, "Use of the discrete Fourier transform in the measurement of frequencies and levels of tones," *Bell Syst. Tech. J.*, vol. 49, pp. 197–228, 1970.
[9] V. K. Jain, W. L. J. Collins, and D. C. Davis, "High-accuracy analog measurements via interpolated FFT," *IEEE Trans. Instrum. Meas.*, vol. IM-28, no. 2, pp. 113–122, Jun. 1979.
[10] J. Schoukens, R. Pintelon, and H. Van Hamme, "The interpolated fast Fourier transform: A comparative study," *IEEE Trans. Instrum. Meas.*, vol. 41, no. 2, pp. 226–232, Apr. 1992.
[11] M. D. Macleod, "Fast nearly ML estimation of the parameters of real or complex single tones or resolved multiple tones," *IEEE Trans. Signal Process.*, vol. 46, no. 1, pp. 141–148, Jan. 1998.
[12] T. Grandke, "Interpolation algorithms for discrete Fourier transforms of weighted signals," *IEEE Trans. Instrum. Meas.*, vol. IM-32, no. 2, pp. 350–355, Jun. 1983.
[13] C. Offelli and D. Petri, "Interpolation techniques for real-time multifrequency waveform analysis," *IEEE Trans. Instrum. Meas.*, vol. 39, no. 1, pp. 106–111, Feb. 1990.
[14] G. Andria, M. Savino, and A. Trotta, "Windows and interpolation algorithms to improve electrical measurement accuracy," *IEEE Trans. Instrum. Meas.*, vol. 38, no. 4, pp. 856–863, Aug. 1989.
[15] E. Jacobsen and P. Kootsookos, "Fast, accurate frequency estimators," *IEEE Signal Process. Mag.*, vol. 24, no. 3, pp. 123–125, May 2007.
[16] B. G. Quinn, "Estimating frequency by interpolation using Fourier coefficients," *IEEE Trans. Signal Process.*, vol. 42, no. 5, pp. 1264–1268, May 1994.
[17] E. Aboutanios and B. Mulgrew, "Iterative frequency estimation by interpolation on Fourier coefficients," *IEEE Trans. Signal Process.*, vol. 53, no. 4, pp. 1237–1242, Apr. 2005.
[18] D. Gallo, R. Langella, and A. Testa, "Desynchronized processing technique for harmonic and interharmonic analysis," *IEEE Trans. Power Del.*, vol. 19, no. 3, pp. 993–1001, Jul. 2004.
[19] C. Liguori, A. Paolillo, and A. Pignotti, "Estimation of signal parameters in the frequency domain in the presence of harmonic interference: A comparative analysis," *IEEE Trans. Instrum. Meas.*, vol. 55, no. 2, pp. 562–569, Apr. 2006.
[20] D. Agrez, "Weighted multipoint interpolated DFT to improve amplitude estimation of multifrequency signal," *IEEE Trans. Instrum. Meas.*, vol. 51, no. 2, pp. 287–292, Apr. 2002.

[21] D. Belega and D. Dallet, "Frequency estimation via weighted multipoint interpolated DFT," *IET Sci., Meas. Technol.*, vol. 2, no. 1, pp. 1–8, Jan. 2008.
[22] B. G. Quinn, "Estimation of frequency, amplitude, and phase from the DFT of a time series," *IEEE Trans. Signal Process.*, vol. 45, no. 3, pp. 814–817, Mar. 1997.
[23] S. Rapuano and F. J. Harris, "An introduction to FFT and time domain windows," *IEEE Instrum. Meas. Mag.*, vol. 10, no. 6, pp. 32–44, Dec. 2007.
[24] I. S. Reljin, B. D. Reljin, and V. D. Papic, "Extremely flat-top windows for harmonic analysis," *IEEE Trans. Instrum. Meas.*, vol. 56, no. 3, pp. 1025–1041, Jun. 2007.
[25] K. F. Chen and Y. F. Li, "Combining the Hanning windowed interpolated FFT in both directions," *Comput. Phys. Commun.*, vol. 178, no. 12, pp. 924–928, Jun. 2008.
[26] K. F. Chen, J. T. Jiang, and S. Crowsen, "Against the long-range spectral leakage of the cosine window family," *Comput. Phys. Commun.*, vol. 180, no. 6, pp. 904–911, Jun. 2009.
[27] X. Z. Yang, H. Y. Li, and K. F. Chen, "Optimally weighted average of the interpolated fast Fourier transform in both directions," *IET Sci., Meas. Technol.*, vol. 3, no. 2, pp. 137–147, Mar. 2009.
[28] D. C. Rife and R. R. Boorstyn, "Single-tone parameter estimation from discrete-time observation," *IEEE Trans. Inf. Theory*, vol. IT-20, no. 5, pp. 591–598, Sep. 1974.
[29] P. Handel, "Properties of the IEEE-STD-1057 four-parameter sine wave fit algorithm," *IEEE Trans. Instrum. Meas.*, vol. 49, no. 6, pp. 1189–1193, Dec. 2000.
[30] D. Agrez, "Improving phase estimation with leakage minimization," *IEEE Trans. Instrum. Meas.*, vol. 54, no. 4, pp. 1347–1353, Aug. 2005.

Kui Fu Chen received the Ph.D. degree in biomedical engineering from Peking Union Medical College, Beijing, China, in 2000.

He was a Postdoctorate with Oregon Health and Science University, Portland, from October 2002 to May 2004, and a Research Associate with the Rehabilitation Institute of Chicago, Chicago, IL, from May 2004 to August 2005. He is currently an Associate Professor with the College of Sciences, China Agricultural University, Beijing. He has published more than 70 peer-reviewed papers.

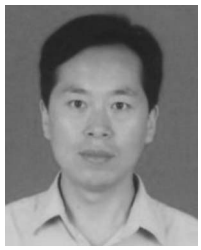

Shu Li Mei received the Ph.D. degree in vehicle engineering from China Agricultural University, Beijing, China, in 2002.

In 2002, he joined Beihang University, Beijing, China, as a Postdoctorate in general and fundamental mechanics. Since 2004, he has been an Associate Professor of computer science and technology with China Agricultural University.